Non-genericity of the Nariai solutions: II. Investigations within the Gowdy class

Florian Beyer
beyer@ann.jussieu.fr

Laboratoire Jacques-Louis Lions
Université Pierre et Marie Curie (Paris 6)
4 Place Jussieu, 75252 Paris, France

Abstract

This is the second of two papers where we study the asymptotics of the generalized Nariai solutions and its relation to the cosmic no-hair conjecture. In the first paper, the author suggested that according to the cosmic no-hair conjecture, the Nariai solutions are non-generic among general solutions of Einstein's field equations in vacuum with a positive cosmological constant. We checked that this is true within the class of spatially homogeneous solutions. In this paper now, we continue these investigations within the spatially inhomogeneous Gowdy case. On the one hand, we are motivated to understand the fundamental question of cosmic no-hair and its dynamical realization in more general classes than the spatially homogeneous case. On the other hand, the results of the first paper suggest that the instability of the Nariai solutions can be exploited to construct and analyze physically interesting cosmological black hole solutions in the Gowdy class, consistent with certain claims by Bousso in the spherically symmetric case. However, in contrast to that, we find that it is not possible to construct cosmological black hole solutions by means of small Gowdy symmetric perturbations of the Nariai solutions and that the dynamics shows a certain new critical behavior. For our investigations, we use the numerical techniques based on spectral methods which we introduced in a previous publication.

1 Introduction

In this work, we are interested in a particular consequence of the cosmic no-hair conjecture [16, 19]. As discussed in our first paper [5], this conjecture suggests that the so-called Nariai solutions are non-generic in the class of cosmological solutions of Einstein's field equations in vacuum

$$G_{\mu\nu} + \Lambda g_{\mu\nu} = 0, \tag{1.1}$$

with a positive cosmological constant Λ, due to its extraordinary asymptotics for large times. Throughout the paper, a cosmological solution means a globally hyperbolic solution of Eq. (1.1) with compact Cauchy surfaces.

In the first paper [5], we analyzed the asymptotics of what we called generalized Nariai solutions. A particular solution in this family is the (standard) Nariai solution [23, 24]. Although these solutions are all isometric locally to the standard Nariai solution, we were motivated to introduce this family for the following reasons. First, their spatially homogeneous perturbations have interesting properties [5]. Second, the approach presented in this paper here makes particular use of the non-standard Nariai solutions in this family. In the following, we often speak of "Nariai solutions", when we mean any generalized Nariai solution. A particular contribution of the first paper was a proof of the outstanding fact that the Nariai solutions do not possess smooth conformal boundaries, a result closely related to the cosmic no-hair picture as explained there. Moreover, we investigated how the expected non-genericity of the Nariai solutions is realized dynamically in the spatially homogeneous class of perturbations. In general, when we speak of a perturbation of a Nariai solutions, we mean a cosmological solution of the fully non-linear Einstein's field equations Eq. (1.1) whose data, on some Cauchy surface, is close to the data on a Cauchy surface of a generalized Nariai solution. By "close" we mean that two data sets should deviate not too much with respect to some reasonable norm in the initial data space. We show in [5] that an arbitrary small spatially homogeneous perturbation of any Nariai solution does either not expand at all in, say, the future, or it expands in a manner consistent with the cosmic no-hair picture by forming a smooth future conformal boundary.

Certainly, the case of spatially homogeneous perturbations is special and it would be interesting to study the instability of the Nariai solutions within more general classes of perturbations. Beyond the problem of cosmic no-hair, however, it is a tempting possibility to exploit our knowledge about the instability in the homogeneous case in order to construct new non-trivial inhomogeneous cosmological black hole solutions. Recall from the results in the first paper [5] that in the spatially homogeneous case, the sign of the initial expansion $H_*^{(0)}$ of the spatial $\mathbb{S}^2$-factor of a perturbation of a Nariai solution controls whether the spatial $\mathbb{S}^2$-factor collapses or expands to the future. Hence, one can expect that by making $H_*^{(0)}$ spatially dependent on the initial hypersurface, we become able to control the *spatially local* behavior of the perturbations. In particular, we should obtain solutions with arbitrary many black hole interiors on the one hand and expanding cosmological regions on the other hand. In principle, we are interested in studying generic inhomogeneous perturbations of the Nariai solutions without any symmetries. However, this is not feasible in practice. A systematic approach would be to reduce the symmetry assumptions step by step. The first systematic step is the spherically symmetric case. Indeed Bousso in [7] claims that arbitrarily complicated spherically symmetric cosmological black hole solutions can be constructed with this approach.

In this paper, we do not consider the spherically symmetric case, but rather proceed with the Gowdy symmetric case. Gowdy symmetric solutions with spatial $\mathbb{T}^3$-topology have been very prominent in the field of mathematical cosmology, and recently, important outstanding problems have been tackled rigorously; see the important work in [26, 27] based on a long list of previous references. However, the Gowdy case with spatial

$\mathbb{S}^1 \times \mathbb{S}^2$-topology (and $\mathbb{S}^3$), which is the relevant case here, has turned out to be more difficult analytically [21, 15, 28]. This is one particular motivation for us to proceed with this class by means of numerical techniques. In fact, we have developed numerical techniques in [6] applicable to the $\mathbb{S}^1 \times \mathbb{S}^2$-Gowdy class, which will be used in this work here. An alternative numerical approach for Gowdy solutions with $\mathbb{S}^1 \times \mathbb{S}^2$-topology can be found in [15]. However, this approach is not applicable directly for the conformal field equations based on orthonormal frames which we have decided to work with. In any case, our results can be hoped to complement the claims in [7] in a physically and technically interesting setting.

In all what follows, we use the same fundamental conventions and assumptions as in the first paper [5].

Our paper is organized as follows. In Section 2, we prepare our investigations. After a short introduction to Gowdy symmetry on $\mathbb{S}^1 \times \mathbb{S}^2$ in Section 2.1, we construct those Gowdy invariant initial data sets in Section 2.2, which will be used to study the perturbations of the Nariai solutions later. For the basic properties of these solutions, we refer to Section 3 of [5]. Then, Section 2.3 of the paper here is devoted to the discussion of certain mean curvature quantities which are analogous to those quantities which control the instability of the Nariai solution in the spatially homogeneous case. In Section 2.4, we present the formulation of Einstein's field equations that we will use for the numerical computations, namely the conformal field equations. We briefly describe the unknown variables in this formulation and fix our choice of gauge. We conclude with a comment about our particular reduction to $1 + 1$. We proceed by giving a quick summary of the numerical infrastructure in Section 2.5. In Section 2.6, we comment on how to compute initial data for the conformal field equations from the data constructed in Section 2.2. Numerically, this is not completely trivial, because the initial data before are based on coordinate components of the metric and hence they run the risk of coordinate singularities when they are transformed to orthonormal frame based data for the conformal field equations. In Section 3.1, we fix and motivate particular initial data sets for the later numerical runs. The central part of the paper is Section 3.2, where we show the numerical evolutions and interpret the results. In Section 3.3, we present further details of a practical nature about the numerical runs and then proceed with an analysis of numerical errors. The paper is concluded with a summary, a discussion of open problems and an outlook in Section 4.

2 Preparations

2.1 Gowdy symmetry on $\mathbb{S}^1 \times \mathbb{S}^2$

We quickly introduce important and relevant facts about Gowdy symmetry on $\mathbb{S}^1 \times \mathbb{S}^2$. General aspects of $\mathrm{U}(1) \times \mathrm{U}(1)$-symmetric solutions of Einstein's field equations were discussed in [17] for the first time and later reconsidered in [9].

Smooth $\mathbf{U}(1)\times\mathbf{U}(1)$-invariant metrics on $\mathbb{S}^1\times\mathbb{S}^2$ Let us introduce coordinates (ρ,θ,ϕ) on $\mathbb{S}^1\times\mathbb{S}^2$, where $\rho\in(0,2\pi)$ is the standard parameter on $\mathbb{S}^1$ and (θ,ϕ) are standard polar coordinates on $\mathbb{S}^2$. The coordinate vector fields ∂_ρ and ∂_ϕ generate a smooth effective action of the group $\mathrm{U}(1)\times\mathrm{U}(1)$ on $\mathbb{S}^1\times\mathbb{S}^2$. Let us consider a smooth Riemannian metric h on $\mathbb{S}^1\times\mathbb{S}^2$ which is invariant under this action. One can parametrize h as

$$h = e^{2\lambda}d\theta^2 + R(e^P d\phi^2 + 2e^P Q d\phi\, d\rho + (e^P Q^2 + e^{-P})d\rho^2). \tag{2.1}$$

In particular, the field ∂_θ can be assumed to be orthogonal to the group orbits everywhere. All functions involved here only depend on θ. For the smoothness of h, it is sufficient and necessary [9] that there are function $\tilde{R}$, $\tilde{P}$ and $\tilde{\lambda}$ so that

$$R = \tilde{R}\sin\theta, \quad P = \tilde{P} + \ln\sin\theta, \quad \lambda = (\tilde{P} + \ln\tilde{R})/2 + \tilde{\lambda}, \tag{2.2a}$$

where $\tilde{R}$, $\tilde{P}$, $\tilde{\lambda}$ and Q are smooth function of $\cos\theta$, and

$$\tilde{\lambda}\big|_{\theta=0,\pi} = 0. \tag{2.2b}$$

Gowdy symmetric spacetimes with spatial $\mathbb{S}^1\times\mathbb{S}^2$-topology Now let us consider a globally hyperbolic spacetime (M,g) foliated with $\mathrm{U}(1)\times\mathrm{U}(1)$-invariant Cauchy surfaces of topology $\mathbb{S}^1\times\mathbb{S}^2$, in the sense that the first and second fundamental form of each surface are invariant under the $\mathrm{U}(1)\times\mathrm{U}(1)$-action before. It has been shown before [9, 10] that this action is orthogonally transitive, i.e. the twist constants

$$c^1 := \epsilon^{\mu\nu\sigma\lambda}\eta^1_\mu\sigma^2_\nu\partial_\sigma\eta^a_\lambda, \quad c^2 := \epsilon^{\mu\nu\sigma\lambda}\eta^1_\mu\sigma^2_\nu\partial_\sigma\sigma^a_\lambda$$

vanish for spatial topology $\mathbb{S}^1\times\mathbb{S}^2$ (or $\mathbb{S}^3$, but not $\mathbb{T}^3$) if this spacetime is a solution of Eq. (1.1). Here all index manipulations are done with the metric g, and ϵ is the volume form of g assuming that the spacetime is orientable. See also [29] for more details. In general, if these constants vanish, a $\mathrm{U}(1)\times\mathrm{U}(1)$-invariant spacetime is called Gowdy spacetime [17]. Thus, all $\mathrm{U}(1)\times\mathrm{U}(1)$-invariant solutions of Eq. (1.1) with spatial topology $\mathbb{S}^1\times\mathbb{S}^2$ (or $\mathbb{S}^3$) are Gowdy solutions.

It is clear that that there exist coordinate gauges which are inconsistent with the assumption, that for all $t = const$-hypersurfaces, the first and second fundamental form are $\mathrm{U}(1)\times\mathrm{U}(1)$-invariant and that the Killing vector fields can be identified with the coordinate vector fields ∂_ρ and ∂_ϕ for all values of the time coordinate t. Most prominent examples of – in this sense – consistent gauges are the so-called areal gauge where one sets $\tilde{R} = t$, and the "conformal time gauge"[1] where the time coordinate t is chosen so that

$$g = -e^{2\lambda}dt^2 + h \tag{2.3}$$

[1]The name "conformal time gauge" must not be confused with the conformal approach described in Section 2.4. This name was chosen because the 2-surfaces orthogonal to the group orbits are explicitly conformally flat.

with h given by Eq. (2.1) together with Eqs. (2.2); for more information see for instance [10]. A further "consistent" choice of gauge is the Gauss gauge. Here the time coordinate t is chosen so that metric g takes the form

$$g = -dt^2 + h \tag{2.4}$$

with the same h as before.

Spatial homogeneity and the Nariai case If (M, g) is spatially homogeneous, it is in particular Gowdy symmetric, and hence the metric takes the following form in the conformal time gauge

$$g = \tilde{R}e^{\tilde{P}}(-dt^2 + d\theta^2 + \sin^2\theta d\phi^2) + \tilde{R}e^{-\tilde{P}}d\rho^2. \tag{2.5}$$

All functions in this metric only depend on t. In this gauge, the generalized Nariai metrics are determined by

$$\tilde{R}(t) = \Phi(t)/\Lambda, \quad \tilde{P}(t) = -\ln\Phi(t). \tag{2.6}$$

2.2 A family of Gowdy symmetric initial data close to Nariai data

Our aim is now to find Gowdy invariant initial data close to the Nariai solution. These will be interpreted as perturbed Nariai data, and the corresponding solutions of the field equations as perturbed Nariai solutions. Our data sets must be solutions of the constraint equations implied by the vacuum Einstein's field equations with $\Lambda > 0$ on a Cauchy surface of $\mathbb{S}^1 \times \mathbb{S}^2$-topology.

Since Gowdy symmetry is generated by the coordinate vector fields ∂_ρ and ∂_ϕ, our initial value problem reduces to a problem on the domain of the coordinates (t, θ) in principle. Let t be the time coordinate of the "conformal time gauge" defined in Eq. (2.3). The constraints are

- Hamiltonian constraint:

$$0 = \frac{1}{4}P'^2 + \frac{1}{4}e^{2P}Q'^2 - \frac{R'^2}{4R^2} + \frac{1}{4}\dot{P}^2 + \frac{1}{4}e^{2P}\dot{Q}^2 - \frac{\dot{R}^2}{4R^2} + e^{2\lambda}\Lambda - \frac{R'\lambda'}{R} + \frac{R''}{R} - \frac{\dot{R}\dot{\lambda}}{R},$$

- Momentum constraint

$$0 = \frac{1}{2}P'\dot{P} + \frac{1}{2}e^{2P}Q'\dot{Q} - \frac{R'\dot{R}}{2R^2} - \frac{\lambda'\dot{R}}{R} - \frac{R'\dot{\lambda}}{R} + \frac{\dot{R}'}{R}.$$

A dot represents a t-derivative and a prime a θ-derivative. We assume that on the initial hypersurface, the action of the Gowdy group is of the standard form, which implies that the quantities R, P, Q, λ must be expressible via Eqs. (2.2). When the new quantities $\tilde{R}$, $\tilde{P}$ and $\tilde{\lambda}$ are substituted into the constraint equations, formally singular terms arise at the coordinate singularities $\theta = 0, \pi$. In this paper, we do not address

the problem of these terms; another future publication will be devoted to such and related issues. In the case $\Lambda = 0$, the corresponding problem arises [15]. For $\Lambda > 0$, however, Eq. (14) in [15] must be substituted by a more complicated condition due to the additional term $e^{2\tilde{\lambda}}\Lambda$. In order to circumvent these problems for the time being as in [15], we are satisfied with a particular family of explicit solutions of the constraints with the properties above for this paper. However, it is clear that such a family of initial data cannot be considered "generic" and hence no strict results about the cosmic no-hair conjecture can be expected. Nevertheless, we see the investigations in this paper as a promising first step.

In all of what follows, we assume $\Lambda = 3$ with loss of generality, since it yields the simplest expressions and makes all quantities dimensionless. We have mentioned before that the functions $\tilde{R}$, $\tilde{P}$, Q and $\tilde{\lambda}$ must be smooth functions of $\cos\theta$, and $\tilde{\lambda}$ has to become zero at $\theta = 0, \pi$. Now, we make a polynomial ansatz for these functions in $z = \cos\theta$, and solve the constraints for the polynomial coefficients matching these conditions. In this way, which requires cumbersome algebra done with Mathematica, we derive the following almost explicit family of Gowdy symmetric solutions of the constraints

$$\tilde{R} = \tilde{R}_*, \qquad \tilde{R}' = \frac{\tilde{R}_*}{\kappa}, \tag{2.7a}$$

$$\tilde{P} = P_* - \frac{\sqrt{3}}{2\kappa}\tilde{N}^{(1)}_\times \sin^2\theta, \qquad \tilde{P}' = \frac{\sqrt{3}}{\kappa}(\Sigma^{(0)}_- - \Sigma^{(1)}_\times \cos^2\theta), \tag{2.7b}$$

$$Q = -\frac{\sqrt{3}}{\kappa}\tilde{N}^{(1)}_\times \int_{-1}^{\cos\theta} e^{-\tilde{P}(z)}dz, \qquad Q' = \frac{\sqrt{3}}{\kappa}\Sigma^{(1)}_\times e^{-\tilde{P}}, \tag{2.7c}$$

$$\tilde{\lambda} = \frac{\sqrt{3}}{4\kappa}\tilde{N}^{(1)}_\times \sin^2\theta, \qquad \tilde{\lambda}' = \frac{\sqrt{3}}{2\kappa}(\sqrt{3}\Sigma^{(2)}_+ - \Sigma^{(1)}_\times)\sin^2\theta. \tag{2.7d}$$

The constants P_*, $\tilde{N}^{(1)}_\times$, $\Sigma^{(2)}_+$ are determined transcendentally by the initial data parameters $(\tilde{R}_*, \kappa, \Sigma^{(0)}_-, \Sigma^{(1)}_\times)$ in the following manner. Let us make the abbreviation

$$C := \frac{1}{\sqrt{3}\,\kappa}\sqrt{\kappa^4 + \left(3(\Sigma^{(1)}_\times)^2 - 6\Sigma^{(0)}_-\Sigma^{(1)}_\times + 2\sqrt{3}\Sigma^{(0)}_-\right)\kappa^2 + 3(\Sigma^{(1)}_\times - \Sigma^{(0)}_-)^2}.$$

Then

$$P_* = \ln\left[\frac{1}{4\tilde{R}_*\kappa^2}\left(\frac{2\kappa^2}{3} - \frac{2C\kappa}{\sqrt{3}} - (\Sigma^{(1)}_\times)^2 - (\Sigma^{(0)}_-)^2 + 2\Sigma^{(1)}_\times\Sigma^{(0)}_- + 1\right)\right],$$

$$\tilde{N}^{(1)}_\times = \frac{\Sigma^{(1)}_\times - \Sigma^{(0)}_-}{\kappa} - C - \frac{\kappa}{\sqrt{3}},$$

$$\Sigma^{(2)}_+ = \frac{3(\Sigma^{(1)}_\times)^2 - 6\Sigma^{(0)}_-\Sigma^{(1)}_\times + 3C\kappa(\Sigma^{(0)}_- - \Sigma^{(1)}_\times) + \Sigma^{(0)}_-\left(\sqrt{3}\kappa^2 + 3\Sigma^{(0)}_-\right)}{3\kappa^2}.$$

The reality conditions on both the root in the definition of C and the logarithm in the definition of P_* imply restrictions for the choice of the (otherwise free) parameters

$(\tilde{R}_*, \kappa, \Sigma_-^{(0)}, \Sigma_\times^{(1)})$ which, however, we do not make explicit now. For the applications later, we always check that these are satisfied without further notice. Let us suppose that all quantities in Eqs. (2.7) are well defined. The only non-explicit expression is the integral for Q when $\Sigma_\times^{(1)} \neq 0$. We compute this integral numerically by approximating the exponential by its truncated Taylor series. This series converges very quickly and in practice, the series can be truncated after a few terms.

Let us also remark that these data are not polarized in general, i.e. the Killing fields cannot be chosen globally orthogonal.

Now, let us identify spatially homogeneous, and in particular Nariai data in our family Eq. (2.7). Writing Eq. (2.5) for the conformal time gauge according to Eq. (2.3), we see that spatial homogeneity implies $\Sigma_\times^{(1)} = \tilde{N}_\times^{(1)} = \Sigma_+^{(2)} = 0$. Using the expressions above, the data are hence spatially homogeneous if and only if

$$\Sigma_-^{(0)} \leq -\frac{\kappa^2}{\sqrt{3}}, \quad \Sigma_\times^{(1)} = 0. \tag{2.8}$$

In particular, $\Sigma_\times^{(1)}$ plays the role of an "inhomogeneity parameter". However, our family of data does not comprise all spatially homogeneous data, in particular not all Nariai data. For any generalized Nariai data, Eq. (2.6) implies

$$\tilde{R}_* = \Phi_*/\Lambda, \quad \kappa = \Phi_*/\Phi_*', \quad \Sigma_-^{(0)} = -1/\sqrt{3}, \quad \Sigma_\times^{(1)} = 0. \tag{2.9}$$

In this case, Eq. (2.8) yields $\kappa^2 \leq 1$, and thus only generalized Nariai solutions with $\sigma_0 \leq 0$ are present in our data.

2.3 Mean curvatures and the expected instability in the Gowdy class

In principle, there is no "canonical" quantity which could play the same role for the instability of the Nariai solutions in the spatially inhomogeneous case as the quantity $H_*^{(0)}$ defined in Section 4.1 in the first paper [5] in the spatially homogeneous case. First, there is no "canonical" foliation of spacetime, and, second, no "geometrically preferred spatial $\mathbb{S}^2$-factor". Here, we choose a Gaussian foliation with time coordinate t; cf. Eq. (2.4). At this stage, we can only hope that at least for small perturbations of the Nariai solutions, the "expansion of the coordinate $\mathbb{S}^2$-factor", which we define now, plays a similar role here as $H_*^{(0)}$; at least these quantities agree for spatially homogeneous perturbations.

On the initial hypersurface, we choose coordinates (ρ, θ, ϕ) as before. By means of the Gauss gauge condition, these spatial coordinates are transported to all $t = const$-hypersurfaces Σ_t. On any Σ_t, a "coordinate $\mathbb{S}^2$-factor" is then a 2-surface diffeomorphic to $\mathbb{S}^2$ determined by $\rho = const$. Since the metric is invariant under translation along ρ, all such 2-surfaces are isometric at a given t. Similarly, we define "coordinate $\mathbb{S}^1$-factors"; note that these 1-surfaces are not isometric on a given Σ_t. The expansions (mean curvatures) associated with these surfaces are defined as follows for a Gauss gauge. Let H be the mean curvature of any $t = const$-hypersurface. Let H_2 be the projection of the

mean curvature vector of a coordinate $\mathbb{S}^2$-factor to ∂_t; this is the quantity we refer to as the "expansion of the coordinate $\mathbb{S}^2$-factor". Similarly, we define H_1 as the "expansion of the coordinate $\mathbb{S}^1$-factor". With the expression Eq. (2.1) for the spatial metric, the following formulas hold

$$H = \frac{3\tilde{R}' + \tilde{R}\left(\tilde{P}' + 2\tilde{\lambda}'\right)}{6\tilde{R}}, \quad H_2 = \frac{\tilde{R}' + \tilde{R}\left(\tilde{P}' + \tilde{\lambda}'\right)}{2\tilde{R}}, \tag{2.10a}$$

$$3H - 2H_2 - H_1 = -\frac{e^{2\tilde{P}} Q \sin^2\theta \left(Q\tilde{P}' + Q'\right)}{1 + e^{2\tilde{P}} Q^2 \sin^2\theta}, \tag{2.10b}$$

where a prime denotes a derivative with respect to Gaussian time[2].

We expect that, as for the quantity $H_*^{(0)}$ in the spatial homogeneous case, the sign of the initial value of H_2 controls whether the solution collapses or expands locally in space and hence plays a particularly important role for the description of the expected instability of the Nariai solutions. Thus we write down the expression for the family of initial data in Eqs. (2.7)

$$\begin{aligned} H_2|_{\text{initial}} =& \frac{1}{4\kappa^3}\Big[3(\Sigma_\times^{(1)} - \Sigma_-^{(0)})^2 - 3\kappa C(\Sigma_\times^{(1)} - \Sigma_-^{(0)}) + \kappa^2(2 - \sqrt{3}\Sigma_\times^{(1)} + 3\sqrt{3}\Sigma_-^{(0)}) \\ & - \left(3(\Sigma_\times^{(1)} - \Sigma_-^{(0)})^2 - 3\kappa C(\Sigma_\times^{(1)} - \Sigma_-^{(0)}) + \sqrt{3}\kappa^2(\Sigma_\times^{(1)} + \Sigma_-^{(0)}\right)\cos^2\theta\Big]. \end{aligned} \tag{2.11}$$

2.4 Formulation of Einstein's field equations

Our numerical approach, based on orthonormal frames for the conformal field equations is discussed in [6, 4] and is briefly summarized in the following paragraphs. The main motivation for using this approach is that the conformal techniques allow us, in principle, to compute the conformally extended solutions including conformal boundaries. Recall that in our setting, smooth conformal boundaries represent the infinite timelike future or past, and hence play a particular role for the cosmic no-hair picture; cf. Section 3.1 in the first paper [5].

The "physical metric", by which we mean a solution of Einstein's field equations, is denoted by $\tilde{g}$, and all corresponding quantities (connection coefficients, curvature tensor components etc.) are marked with a tilde[3]. The so-called "conformal metric" on the conformal compactification is denoted by g; all corresponding quantities are written without a tilde. Both metrics are related by the expression $g = \Omega^2\tilde{g}$, where $\Omega > 0$ is a conformal factor. We cannot give further explanations here; some more details are listed in the first paper [5], and a comprehensive review is in [12].

We will use Friedrich's general conformal field equations in a special conformal Gauss gauge [11, 12, 22, 3, 4]. In turns out that up to a rescaling of the time coordinate t of

[2]Recall that, by contrast, a prime denotes a derivative with respect to the time coordinate in conformal time gauge in Eqs. (2.7).

[3]Be aware that this is the opposite notation than in [5]; there, all quantities defined with respect to the conformal metric are marked with a tilde.

this gauge, it is equivalent to a physical Gauss gauge (defined with respect to $\tilde{g}$) with time coordinate $\tilde{t}$. For $\Lambda = 3$, the rescaling has the form

$$\tilde{t} = \ln \frac{t}{2-t}.$$

If a smooth compact past conformal boundary $\mathcal{J}^-$ exists, and if the solution extends to the conformal boundary in this gauge, then $\mathcal{J}^-$ equals the $t = 0$-hypersurface where $\tilde{t} \to -\infty$. Under analogous conditions, $\mathcal{J}^+$ is represented by the $t = 2$-hypersurface where $\tilde{t} \to \infty$.

Now we write the evolution equations and list the unknowns. We always assume $\Lambda = 3$ in order to obtain the simplest expressions as possible. Among the unknown fields is a smooth frame $\{e_i\}$, which is orthonormal with respect to g, and which we represent as follows. Due to our gauge choice, we can fix

$$e_0 = \partial_t \tag{2.12a}$$

which is henceforth the future directed unit normal, with respect to g, of the $t = const$-hypersurfaces. Furthermore, we write

$$e_a = e_a{}^b V_b, \tag{2.12b}$$

where $(e_a{}^b)$ is a smooth 3×3-matrix valued function with non-vanishing determinant on $\mathbb{S}^1 \times \mathbb{S}^2$. Let us define

$$W_1 = \sin\phi\partial_\theta + \cos\phi\cot\theta\partial_\phi, \quad W_2 = \cos\phi\partial_\theta - \sin\phi\cot\theta\partial_\phi, \quad W_3 = \partial_\phi, \tag{2.13}$$

and from those the vector fields

$$\begin{aligned} &V_1 = 2(-\sin\theta\cos\phi\,\partial_\rho + W_1), \quad V_2 = 2(\sin\theta\sin\phi\,\partial_\rho + W_2), \\ &V_3 = 2(\cos\theta\,\partial_\rho + W_3). \end{aligned} \tag{2.14}$$

The factors 2 are chosen for later convenience. It turns out that $\{V_a\}$ forms a smooth global frame on $\mathbb{S}^1 \times \mathbb{S}^2$.

Having fixed the residual gauge initial data, as described in [3], a hyperbolic reduction of the general conformal field equations is given by

$$\partial_t e_a{}^c = -\chi_a{}^b e_b{}^c, \tag{2.15a}$$

$$\partial_t \chi_{ab} = -\chi_a{}^c \chi_{cb} - \Omega E_{ab} + L_{ab}, \tag{2.15b}$$

$$\partial_t \Gamma_a{}^b{}_c = -\chi_a{}^d \Gamma_d{}^b{}_c + \Omega B_{ad} \epsilon^{b\ d}_{\ c}, \tag{2.15c}$$

$$\partial_t L_{ab} = -\partial_t\Omega\, E_{ab} - \chi_a{}^c L_{cb}, \tag{2.15d}$$

$$\partial_t E_{fe} - D_{e_c} B_{a(f} \epsilon^{ac}{}_{e)} = -2\chi_c{}^c E_{fe} + 3\chi_{(e}{}^c E_{f)c} - \chi_c{}^b E_b{}^c g_{ef}, \tag{2.15e}$$

$$\partial_t B_{fe} + D_{e_c} E_{a(f} \epsilon^{ac}{}_{e)} = -2\chi_c{}^c B_{fe} + 3\chi_{(e}{}^c B_{f)c} - \chi_c{}^b B_b{}^c g_{ef}, \tag{2.15f}$$

$$\Omega(t) = \frac{1}{2}\, t\,(2-t), \tag{2.15g}$$

for the unknowns

$$u = \left(e_a{}^b, \chi_{ab}, \Gamma_a{}^b{}_c, L_{ab}, E_{fe}, B_{fe} \right). \tag{2.15h}$$

The unknowns u are the spatial components $e_a{}^b$ of a smooth frame field $\{e_i\}$ as in Eq. (2.12), the spatial frame components of the second fundamental form χ_{ab} defined with respect to e_0, the spatial connection coefficients $\Gamma_a{}^b{}_c$, given by $\Gamma_a{}^b{}_c e_b = \nabla_{e_a} e_c - \chi_{ac} e_0$ where ∇ is the Levi-Civita covariant derivative operator of the conformal metric g, the spatial frame components of the Schouten tensor L_{ab}, which is related to the Ricci tensor of the conformal metric by

$$L_{\mu\nu} = R_{\mu\nu}/2 - g_{\mu\nu} g^{\rho\sigma} R_{\rho\sigma}/12,$$

and the spatial frame components of the electric and magnetic parts of the rescaled conformal Weyl tensor E_{ab} and B_{ab} [12, 14], defined with respect to e_0. Because the timelike frame field e_0 is hypersurface orthogonal, χ_{ab} is a symmetric tensor field. In order to avoid confusion, we point out that, in general, the conformal factor Ω is part of the unknowns in Friedrich's formulation of the CFE. However, for vacuum with arbitrary Λ and for arbitrary conformal Gauss gauges, it is possible to integrate its evolution equation explicitly [11], so that Ω takes the explicit form Eq. (2.15g) for our choice of gauge. We note that, E_{ab} and B_{ab} are tracefree by definition. Hence we can get rid of one of the components of each tensor, for instance by substituting $E_{33} = -E_{11} - E_{22}$; we do the same for the magnetic part. The evolution equations Eqs. (2.15e) and (2.15f) of E_{ab} and B_{ab} are derived from the Bianchi system [12]. In our gauge, the constraint equations implied by the Bianchi system take the form

$$D_{e_c} E^c{}_e - \epsilon^{ab}{}_e B_{da} \chi_b{}^d = 0, \quad D_{e_c} B^c{}_e + \epsilon^{ab}{}_e E_{da} \chi_b{}^d = 0. \tag{2.16}$$

Here, ϵ_{abc} is the totally antisymmetric symbol with $\epsilon_{123} = 1$, and indices are shifted by means of the conformal metric. The other constraints of the full system above are equally important, but are ignored for the presentation here. Note that in Eqs. (2.15e), (2.15f) and (2.16), the fields $\{e_a\}$ are henceforth considered as spatial differential operators, using Eq. (2.12) and writing the fields $\{V_a\}$ as differential operators in terms of coordinates according to Eq. (2.14) and (2.13). Interpreted as partial differential equations, these evolution equations are symmetric hyperbolic and the initial value problem is well-posed. Further discussions of the above evolution system and the quantities involved can be found in the references above.

Friedrich's CFE allow us to use $\mathcal{J}^+$, i.e. the $t = 2$-surface (or in the same way $\mathcal{J}^-$), as the initial hypersurface. This particular initial value problem was considered in [4]. However, in our present application, not all solutions of interest have smooth conformal boundaries. In order not to exclude those solutions, we choose the $t = 1$-hypersurface as the initial hypersurface, which is a standard Cauchy surface. The hope is that this setup allows us to compute the complete solution including the conformal boundary if it exists.

It is a standard result that there exist no globally smooth frames on $\mathbb{S}^1 \times \mathbb{S}^2$ with the property that each frame vector field has vanishing Lie brackets with both Gowdy Killing

vector fields ∂_ρ and ∂_ϕ. The reason is given for instance in [6]. It is only possible to find a frame whose Lie brackets vanish for one of the two Killing vector fields, say, ∂_ρ. This, however, has the consequence that the frame components of all tensor fields derived from a Gowdy invariant metric g depend on the coordinate ϕ in a non-trivial manner. In order to reduce the evolution equations based on such a frame to $1+1$ dimensions nevertheless, we can do the following [6]. It turns out to be possible to evaluate the ϕ-derivative of every relevant unknown at, say, $\phi = 0$ algebraically in terms of the unknowns. Then one can write an evolution system which only involves θ-derivatives in space by substituting all ϕ-derivatives with these algebraic expressions. The resulting system, which we called $1+1$-system in [6] in the case of spatial $\mathbb{S}^3$-topology, is symmetric hyperbolic for the conformal field equations in our gauge. It follows from the discussion in Section A, that a similar reduction to $1+1$ is possible for spatial $\mathbb{S}^1 \times \mathbb{S}^2$-topology. The resulting system of equations is used exclusively in all of what follows in this paper.

2.5 Numerical infrastructure

It follows from Section A that for Gowdy symmetry, spatial $\mathbb{S}^1 \times \mathbb{S}^2$- and $\mathbb{S}^3$-topology have the same representation. Basically, we only need to substitute the Euler coordinates (χ, ρ_1, ρ_2) in the $\mathbb{S}^3$-case defined in Eqs. (A.2) and (A.4) by the coordinates (θ, ϕ, ρ) in the $\mathbb{S}^1 \times \mathbb{S}^2$-case, and the reference frame $\{Y_a\}$ defined in Eqs. (A.3) by the $\{V_a\}$ mentioned before. Then, it is possible to use the same numerical technique as that which was worked out originally for spatial $\mathbb{S}^3$-topology in [6].

Let us repeat quickly the main ingredients of this code. By means of the Euler coordinates of $\mathbb{S}^3$, it is possible transport all geometric quantities and hence Einstein's field equations themselves from $\mathbb{S}^3$ to $\mathbb{T}^3$; loosely speaking, we make "all spatial directions periodic". It is clear that such a map must be singular at some places. However, it is possible to analyze the behavior of Fourier series at the singular places and to compute the formally singular terms in the equations explicitly. Hence, it is not only natural to use Fourier based pseudospectral spatial discretization due to the periodicity in each spatial direction on $\mathbb{T}^3$ here, but it also allows to regularize the formally singular terms in spectral space. This is the motivation for choosing spectral discretization in space. Nevertheless, a scheme to enforce "boundary conditions" [6] can be necessary in practice to guarantee the numerical smoothness and stability. We come back to this when we present our results in Section 3.

For the time discretization, we use the method of lines. In this work, all numerical results were obtained with the adaptive 5th-order "embedded" Runge Kutta scheme from [25] unless noted otherwise.

2.6 Numerical computation of the initial data for the CFE

In Section 2.2, we constructed initial data for the functions $\tilde{R}$, $\tilde{P}$, Q and $\tilde{\lambda}$. Now we fix the initial value of the frame, i.e. the components $e_a{}^b$ in Eq. (2.12), and compute the corresponding initial values of u in Eq. (2.15h).

We choose the initial value of ${e_a}^b$ as follows. For the family of initial data constructed in Section 2.2, consider the frame $\{V_a\}$ in Eq. (2.14) and perform a Gram-Schmidt orthonormalization with respect to the initial conformal 3-metric. More precisely, we construct the matrix $({e_a}^b)$ from Eq. (2.12) as an upper triangular matrix. For instance, this means that e_3 and V_3 are collinear initially. Of course there is a great freedom of choosing frames, and this choice is just one possibility. Note that for the following, no time derivative of ${e_a}^b$ at the initial time $t = 1$ needs to be prescribed.

Now we comment on the computation of u Eq. (2.15h) from these data. The data in Section 2.2 yield all spatial derivatives of the initial metric components and the first time derivatives. However, in order to compute u at the initial time $t = 1$ from these data, we also need second time derivatives of the data. We calculate these by imposing the evolution equations of Einstein's field equations at $t = 1$. We decided to perform all the computations numerically. Note that for this, the metric functions of the initial data in Section 2.2 yield formally singular terms at $\theta = 0, \pi$. However, we are able to compute these formally singular terms numerically by applying the spectral approach which was described above in the context of the evolution equations. In practice, we find that this allows us to resolve the data u with high accuracy. It turns out that machine round-off errors, i.e. errors introduced by the finite number representation in the computer, often yield the largest error contributions here. This is true in particular when the standard "double precision" with round-off errors of order 10^{-16} on Intel processors is used. Hence, we decided to compute the initial data with "quad precision" of the Intel Fortran compiler [20], where numbers are represented with roughly 32 digits, but which is software emulated and hence relatively slow. For the evolution, we switch back to double precision. All our numerical computations presented here have been obtained in this way.

3 Results

3.1 Choice of perturbed data

Let us proceed by explaining our particular choices of initial data for the following numerical results. We present only perturbations of one generalized Nariai solution given by $\tilde{R}_* = 1.0$, $\kappa = 0.5$ here; cf. Eq. (2.9). In order to perturb these Nariai data in an interesting manner, we choose the inhomogeneity parameter $\Sigma_\times^{(1)}$ in Eq. (2.7) as non-zero, but small, and furthermore introduce a small non-zero parameter μ by

$$\Sigma_-^{(0)} = -1/\sqrt{3} + \mu.$$

For the value $\mu = \Sigma_\times^{(1)} = 0$, the data reduce to Nariai data according to Eq. (2.9). In all of what follows, we show the numerical results for three initial data sets given by

$$\mu = 0.0004667, \quad 0.0004800, \quad 0.0005000,$$

and $\Sigma_\times^{(1)} = 4{\cdot}10^{-4}$ in all these three cases. These choices are motivated as follows. On the one hand, we want to focus on "small perturbations" as a first step in order to study the

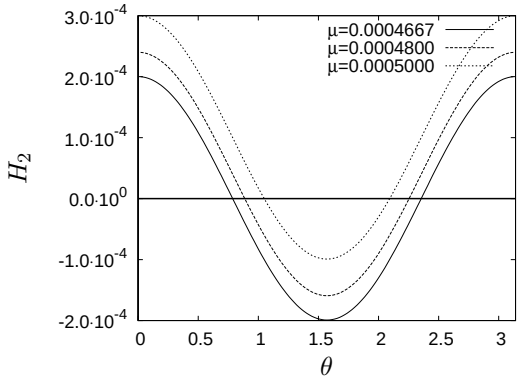

Fig. 1: Initial spatial dependence of H_2 for the three initial data sets considered here.

instability of the Nariai solution carefully. We believe that the choice of the parameters above is consistent with this. Indeed, we have experimented with other values of these parameters. In particular in a large range of values for $\Sigma_\times^{(1)}$, there is no qualitative change in the results that follow. When we go to "very large" values $\Sigma_\times^{(1)} \sim 10^{-1}$, then a different phenomenology occurs; this interesting aspect is currently under investigation and will not be presented in this paper. When we, however, go to even smaller values of $\Sigma_\times^{(1)}$, we get problems with numerical accuracy. Numerical errors in our runs are discussed in Section 3.3. We remark that in this case of small perturbations, a linearization of the field equations around the unperturbed Nariai solution can be a reasonable approximation. This is currently work in progress, but will not be presented here; indeed, all numerical results that follow are based on the full non-linear field equations.

In any case, smallness of the parameters is not the only motivation for our particular choices of data above. Recall that we expect that the instability of the Nariai solution can be exploited to construct cosmological black hole solutions. Our expectation is that this instability is controlled by the sign of the initial value of H_2. For our choices of parameters, H_2 has positive and negative parts according to Eq. (2.11), see Fig. 1. Our expectation for these data sets is hence that in the future, all these solutions collapse and form the interior of a cosmological black hole solution at those spatial places where $H_2 < 0$ initially, i.e. close to the equator of the spatial $\mathbb{S}^2$-factor, and expand and form the cosmological region with a smooth piece of $\mathcal{J}^+$ at those spatial places where $H_2 > 0$ initially, i.e. at the poles of the spatial $\mathbb{S}^2$-factor. Changing the value of μ with fixed $\Sigma_\times^{(1)}$ shifts the initial spatial profiles of H_2 "vertically" in Fig. 1 leaving the shape and the amplitude of the curves approximately invariant. Due to this, we expect that the larger μ is, the "smaller" should be the black hole region of the resulting solution.

3.2 The numerical results

Now we present our numerical results based on these data sets; practical details and a discussion of numerical errors are given afterwards in Section 3.3.

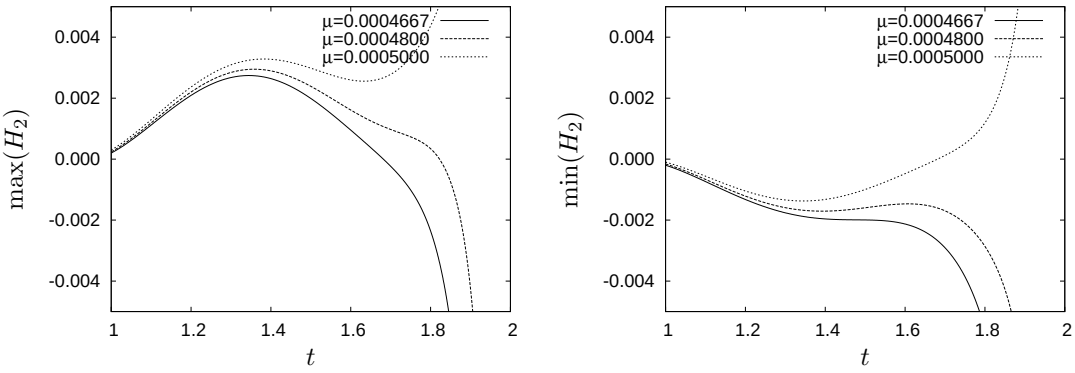

Fig. 2: Spatial minimum and maximum of H_2 vs. time.

Future evolution The horizontal axes in the plots in Fig. 2 represent the time coordinate t; recall that the initial hypersurface corresponds to $t = 1$, and $t = 2$ would correspond to the infinite timelike future. Hence, these plots show the future evolution of H_2 for our three initial data sets. On the vertical axis, we show the maximum and minimum values, respectively, of H_2 at any given time t. In the early phase of the evolution, the solution behaves in accordance with our expectations. Basically, the expansion of the coordinate $\mathbb{S}^2$-factor given by H_2 becomes more and more positive where it is positive initially, namely at the maximum at the poles of the 2-sphere, see again Fig. 1. Furthermore, it becomes more and more negative where it is negative initially, namely at the minimum at the equator of $\mathbb{S}^2$. However, at a time $t \approx 1.3$, the behavior changes completely. The spatial profiles of H_2 start to become "flatter" in the sense that the maximal value of H_2 becomes smaller and the minimal value larger with increasing t, as can be seen from the figure. Eventually the solutions "make a decision" whether the coordinate $\mathbb{S}^2$-factor expands or collapses indefinitely *globally* in space. We give more evidence for this in a moment.

We do not understand the mechanism underlying this phenomenon yet. We hope to be able to to shed further light on this by means of the linearization of the problem in future work. In any case, the numerical results suggest that there is a new instability and a new critical solution, in addition to the expected instability of the Nariai solutions. That is, there must be a critical value μ_c of μ in the interval $(0.00048, 0.0005)$. For $\mu < \mu_c$, the solution collapses eventually, and for $\mu > \mu_c$, expands globally in space. It would be interesting research to identify the critical solution and to study whether critical phenomena, which play such an important role [8] for the critical collapse of black holes, also occur here. In any case, it is an interesting unexpected result that it does not seem possible to construct cosmological black hole solutions for small Gowdy symmetric perturbations of the Nariai solution, in contrast to the claims in [7] for the spherically symmetric case.

We present further evidence for our interpretation of the numerical results now. For

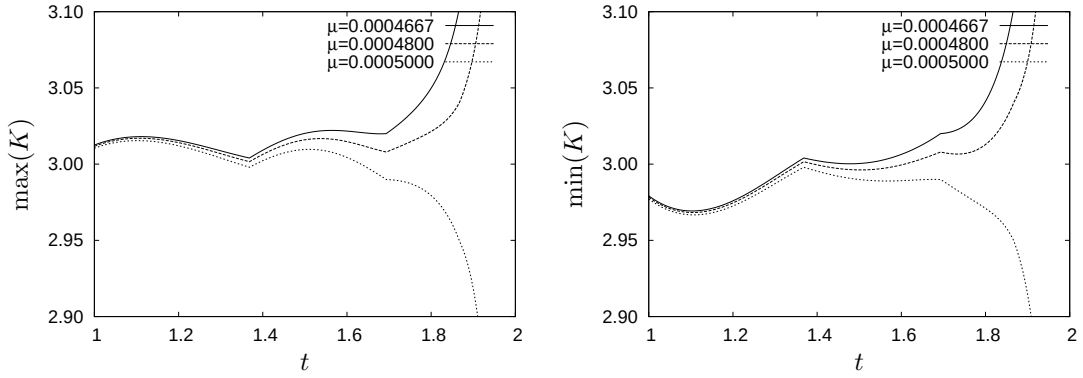

Fig. 3: Spatial minimum and maximum the Kretschmann scalar K vs. time.

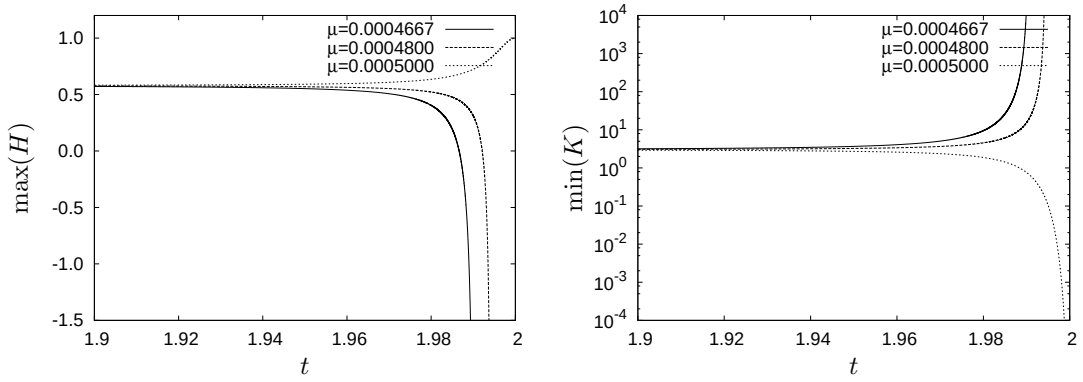

Fig. 4: Future late time behavior.

this, consider the plots in Fig. 3 for the Kretschmann scalar

$$K := \tilde{R}_{\mu\nu\rho\sigma}\tilde{R}^{\mu\nu\rho\sigma},$$

where $\tilde{R}_{\mu\nu\rho\sigma}$ is the Riemann tensor of the physical metric $\tilde{g}$. The curves are consistent with what we have just said, and confirm in particular that the collapse or expansion takes place *globally* in space eventually. The kinks in these curves can be explained as follows. The spatial profiles of the Kretschmann scalar in our evolutions have several local extrema in space which "compete" to become the global extremum.

All the plots so far focus on the early time behavior of the solutions due to the choice of scales on the axes. Now let us look at Fig. 4, which focuses on the evolutions at late times. We note that on these scales, the curves of the maxima and minima of the quantities are not distinguishable and hence we only show one. In the first picture, we show the Hubble scalar H, cf. Eqs. (2.10). In the eventually expanding case given by $\mu = 0.0005$, we can show that the solution develops a smooth $\mathcal{J}^+$ numerically. This is consistent with (but not implied by) the fact that H converges to the value 1 at $t = 2$ in the plot. Recall the discussion of the behavior of H at $\mathcal{J}^+$ in Section 3 of the first

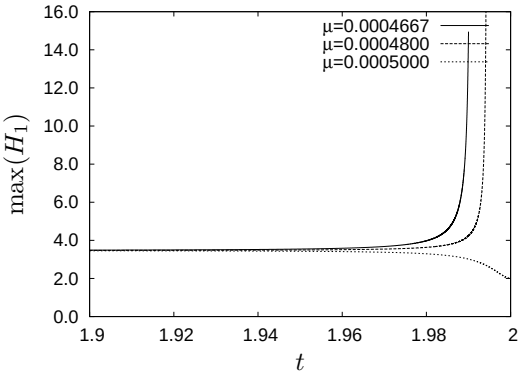

Fig. 5: Future evolution of the expansion of $\mathbb{S}^1$-factor.

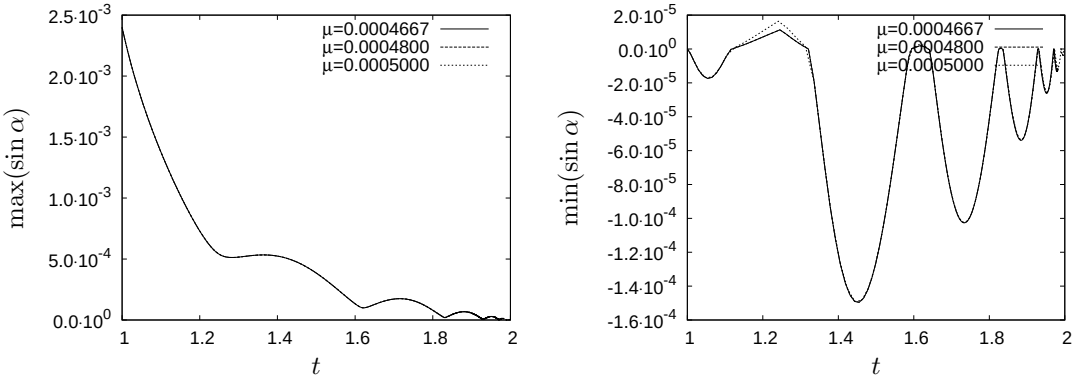

Fig. 6: Future evolution of the angle between the $\mathbb{S}^1$- and the normal of the $\mathbb{S}^2$-factor.

paper [5] for the case $\Lambda = 3$. For the other two solutions, these plots confirm that they collapse indefinitely. This follows from a singularity theorem [2], because in both cases, H eventually becomes smaller than -1. The second plot in Fig. 4 shows K versus t, and it reinforces our previous statement that the curvature of the "collapsing" solutions blows up everywhere in space eventually.

Let us finish this part with a discussion of the evolution of other aspects of the geometry. In Fig. 5, we see the evolution of H_1, cf. Eqs. (2.10), i.e. the expansion of the coordinate $\mathbb{S}^1$-factor. According to this plot, we conjecture that the two collapsing solutions form a singularity of cigar type [29], in the same way as in the spatially homogeneous case [5]. In Fig. 6, we show the maximum and minimum value of $\sin\alpha$, where the angle α is defined as follows. At a given time $t = const$ and spatial point, α is the angle between the vector ∂_ρ and the normal vector of the coordinate $\mathbb{S}^2$-factor within the $t = const$-surface. The plots suggest that α approaches zero eventually. Hence, loosely speaking, the Gowdy solutions become more and more polarized. Again, we do not understand the mechanisms underlying these curves and hope that a linearization will shed further light on this. Since the curves for the three solutions are almost indis-

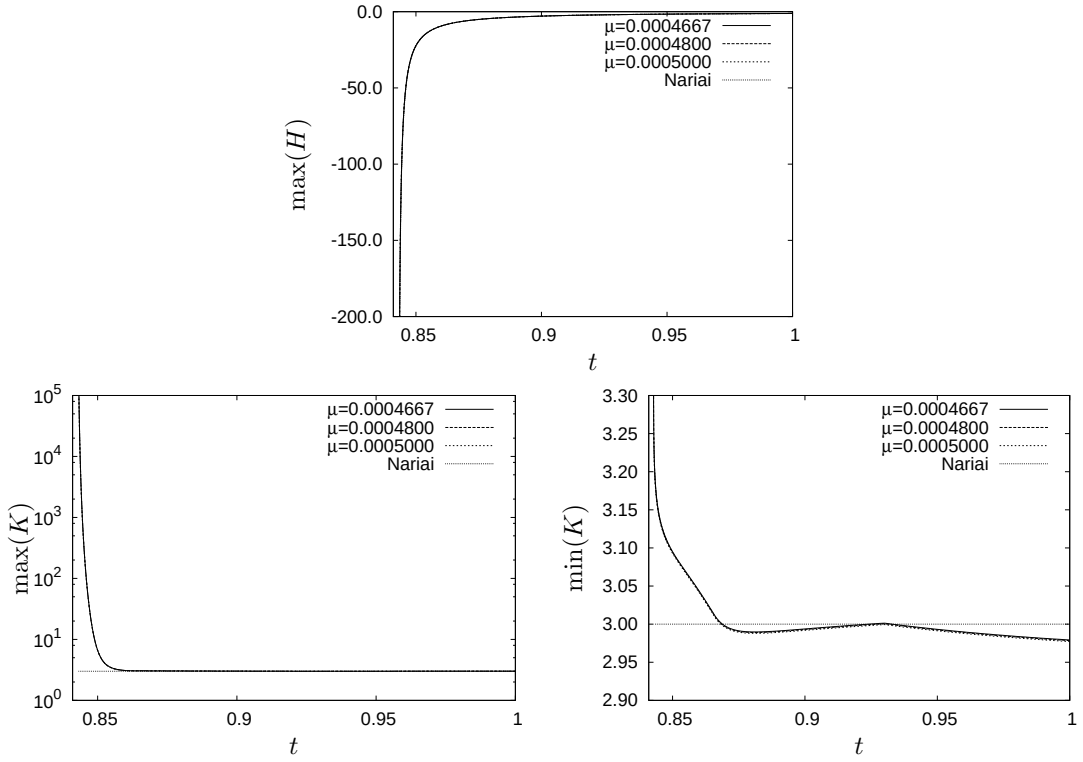

Fig. 7: Past evolution.

tinguishable, it is a natural question whether this behavior is universal in our class of solutions.

Past evolution For completeness, let us proceed with the evolution in the past time direction, and recall from the discussion in the first paper [5] that the unperturbed Nariai solutions with $\sigma_0 < 0$ form a Cauchy horizon in the past. There is additional motivation from the strong cosmic censorship issue [1] to understand what happens to this horizon under our perturbations. Because we consider the past time direction now, the initial hypersurface given by $t = 1$ is on the right of the following plots, and the past evolutions take place to the left. In the first plot of Fig. 7, we show the maximum of the Hubble scalar H for our three cases of initial data together with the corresponding curve of the unperturbed Nariai solution. Again, corresponding curves of the minima are not distinguishable on these scales. We see that the four curves in the plot are almost the same, and hence all four cases collapse in the same way to the past. Do the perturbed solutions hence also develop a Cauchy horizon in the past? The second and third plot in Fig. 7 suggest that this is not the case, as the curvature blows up uniformly for all perturbed solutions. We stress that the numerical results for the minimum of the Kretschmann scalar are not conclusive yet, since the value of $\min(K)$ is still relatively small when the runs were stopped. Nevertheless, first signs of curvature blow up are

direction	μ	N_0	N_1	μ	h_0	h_1	h_{min}	η	t_1
future	0.0004667	300	300	10^{-10}	10^{-3}	10^{-7}	10^{-7}	10^{-15}	1.990
future	0.0004800	300	300	10^{-10}	10^{-3}	10^{-7}	10^{-7}	10^{-15}	1.994
future	0.0005000	200	200	10^{-10}	10^{-3}	10^{-6}	10^{-6}	10^{-14}	2.000
past	0.0004667	200	300	10^{-11}	10^{-3}	10^{-6}	10^{-6}	10^{-14}	0.842
past	0.0004800	200	300	10^{-11}	10^{-3}	10^{-6}	10^{-6}	10^{-14}	0.842
past	0.0005000	200	300	10^{-11}	10^{-3}	10^{-6}	10^{-6}	10^{-14}	0.842

Table 1: Numerical parameters for the runs presented in Section 3.2.

apparent. Our observations in [4] were quite similar, and $\min(K)$ often blew up much less than $\max(K)$ close to a singularity. It is expected that this is not a geometrical phenomenon, but rather caused by the choice of the Gauss gauge, as we discuss there.

3.3 Practical details about the runs and numerical errors

Further technical details Our general numerical setup has been described in Section 2.5. In Table 1 now, we list more technical details about the runs in the previous section. The quantities N_0, N_1 and μ are related to the spatial resolution. Our numerical runs use the simple spatial adaption technique described in [6]. After some experiments, the quantity χ_{22} was chosen as the reference variable. The threshold value for the spatial adaption is called μ, the initial number of spatial grid points is N_0, and the number of spatial grid points at the stop time t_1 is referred to as N_1. The following columns in the table describe the time discretization. We use the 5th-order "embedded" adaptive Runge Kutta scheme with control parameter η. This parameter was introduced in [6] in order to control the desired accuracy of the time integration; the lower its value is, the smaller are the time steps chosen by the adaption algorithm.

Furthermore, h_0 is the initial time step and h_1 is the time step at the stop time t_1. In order to prevent the code from reaching unpractically small values of h, the adaption is switched off when h goes below h_{min}. One sees that for all the runs, this minimum value was reached eventually. Note that all numbers in the table are rounded.

Numerical errors and convergence Prior to the numerical runs in the previous section, we made further tests of the code in addition to those in [6]. The choice of orthonormal frame in Section 2.6 has the consequence that even spatially homogeneous solutions "appear inhomogeneous", in the sense that many resulting unknown tensor components depend on the spatial coordinates. Spatially homogeneous solutions hence yield a non-trivial test case for the code. These tests showed that the code is able to reproduce these solutions with promisingly small errors, in particular the Nariai solution itself.

In order to give the reader an impression of the size of numerical errors in the results in the previous section, let us redo the run for the initial data set $\mu = 0.00048$ and $\Sigma_\times^{(1)} = 4 \cdot 10^{-4}$ to the future with other resolutions than in Table 1. In order to

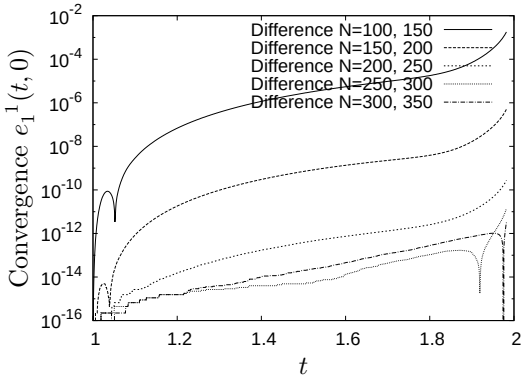

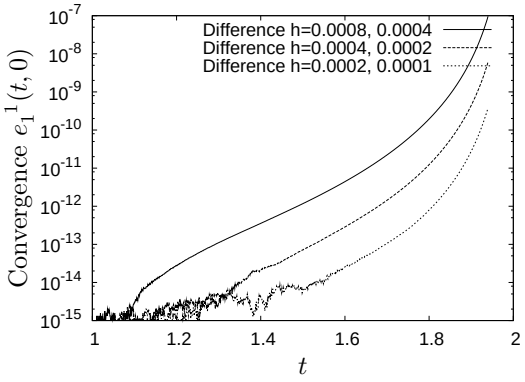

Fig. 8: Spatial convergence for $\mu = 0.00048$. Fig. 9: Time convergence for $\mu = 0.00048$.

study convergence more cleanly, let us switch off all adaption techniques for this. First, consider Fig. 8. For the same initial data, we made six runs with the spatial resolutions $N = 100$, 150, 200, 250, 300 and 350, and fixed size of time step $h = 10^{-4}$. The figure shows the absolute values of the differences of two successive runs for the quantity ${e_1}^1$ at $\theta = 0$ versus time t. We note that we have looked at other variables and seen the same results qualitatively. The absolute size of these differences can be interpreted as a measure for the size of the absolute pure numerical error for a given spatial resolution N (or equivalently spectral truncation) on the one hand. On the other hand, since these errors get smaller dramatically for increasing N, we have demonstrated convergence of the error in our numerical results. Up to $N \approx 300$, the numerical errors in these runs are hence dominated by the spectral discretization. Increasing N further, does not decrease the numerical error, and other types of errors become dominant, in particular the errors given by the time discretization and machine round-off errors. The plot also allows us to quantify the rate of convergence. For resolutions smaller than $N \approx 250$, we find that 50 additional grid points decrease the error by a factor of approximately 3000. This shows that the convergence is exponential in this regime, and hence confirms that our numerical techniques are reliable and the numerical errors in our results in Section 3.2 are small. The fact that spatial resolutions $N \approx 300$ are necessary in order to make spatial discretization errors smaller than other errors even at early times, when the solutions are very smooth in space in principle, shows that our choice of frame is not optimal. However, the fact that we see such a nice convergence for a quantity evaluated at the coordinate singularity $\theta = 0$ provides particular evidence that our numerical regularization of the coordinate singularities mentioned in Section 2.5 works well.

In Fig. 9, we show the same for *fixed* spatial resolution $N = 300$ and the following time resolutions: $h = 8 \cdot 10^{-4}$, $4 \cdot 10^{-4}$, $2 \cdot 10^{-4}$ and $1 \cdot 10^{-4}$. As mentioned earlier, the errors given by the spatial discretization should be negligible for $N = 300$. Note, that here, instead of the adaptive 5th order Runge Kutta scheme, we use the standard 4th order Runge Kutta scheme. The figure confirms 4th order convergence of the errors as long as those are dominated by time discretization. This is the case in particular for

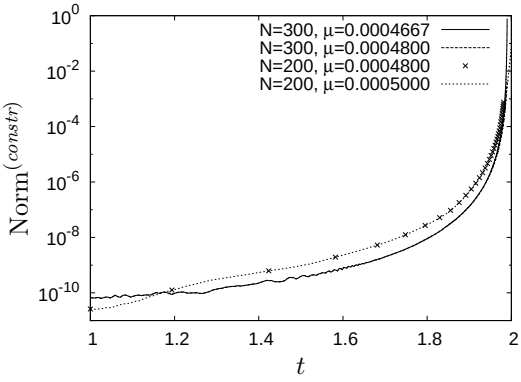

Fig. 10: Violation of the constraints.

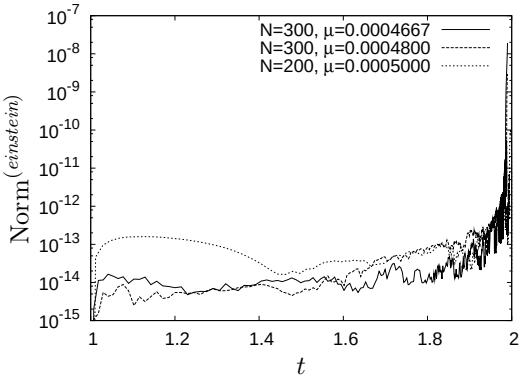

Fig. 11: Violation of Einstein's field eqs.

later evolution times. At very early times, however, the errors are strongly influenced by the machine round-off errors and so barely converge with increasing resolution. If we decreased h even further, the errors would be more and more dominated by round-off errors for longer and longer evolution times and convergence would be lost. Again, all this confirms that our numerical techniques are reliable and the numerical errors in our results in Section 3.2 are well understood and small.

For the discussion of other important error quantities, we introduce the following definitions from [6, 4]. First, we define

$$\mathrm{Norm}^{(einstein)}(t) := \left\| (\tilde{R}_{ij} - \lambda \tilde{g}_{ij})/\Omega \right\|_{L^1(\Sigma_t)},$$

with the physical Ricci tensor $\tilde{R}_{ij}$ evaluated algebraically from the conformal Schouten tensor L_{ij} and derivatives of the conformal factor Ω. The spatial slice at time t is referred to as Σ_t here. The indices involved in this expression are defined with respect to the physical orthonormal frame given by $\tilde{e}_i = \Omega e_i$, and we sum over the L^1-norms of each component. Hence, this norm yields a measure of how well the numerical solution satisfies Einstein's field equations Eq. (1.1). Second, let us define $\mathrm{Norm}^{(constr)}$ as the L^1-norm of the sum of the absolute values of each of the six components of the left hand sides of Eqs. (2.16) at a given instant of time t. For the definition of the norm $\mathrm{Norm}^{(BC)}$, we again refer to [6]. The smoothness of the solution implies a certain behavior of all unknowns in our evolution problem at the coordinate singularities at $\theta = 0, \pi$, and the quantity $\mathrm{Norm}^{(BC)}$ is the sum of the absolute values of all quantities, that, in line with this behavior, should vanish at $\theta = 0, \pi$ at a given time of the evolution.

These norms are used in the following. In addition to the pure numerical errors of the type discussed above, numerical relativity is plagued with the "continuum instability" of the constraint hypersurface in general when the constraints are propagated freely. We hence stress that this is not a particular problem of our numerical investigations here. For some evolution systems, one is able to control the constraint behavior slightly [18], but a general solution to this fundamental problem has not yet been found. When the evolution is started with an arbitrary small violation of the constraints, then typically,

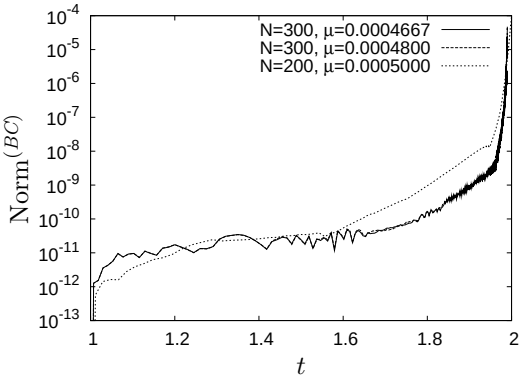

Fig. 12: Violation of boundary conditions.

these violations grow exponentially, or even blow up after finite time, even for the continuum (i.e. non-discretized) equations [13]. In Fig. 10, we see the constraint violations for the runs to the future of the previous section. In addition, we show the constraint propagation for the case $\mu = 0.00048$ and $\Sigma_{\times}^{(1)} = 4 \cdot 10^{-4}$ with the same numerical parameters as for the case $\mu = 0.0005$ from Table 1. In accordance with typical numerical runs, we see that the constraint violations grow strongly during the evolution, almost in the same way whether the solutions collapse or expand eventually. Increasing the initial spatial resolution leads to higher initial constraint violations due to initially higher machine round-off errors. Nonetheless, the plot suggests that the constraint violations decrease once the discretization errors become dominant. This positive result is consistent with our observations in [4], and demonstrates that the constraint violations can be controlled and kept close to the continuum evolution of the constraints for arbitrary large evolution times as long as the errors are dominated by discretization and not by machine round-off errors. As discussed above, for the continuum equations, the initial value of the constraint violation is of fundamental importance. We have tested this for $N = 300$ in the following way, as we do not show here. We have repeated some of the runs before with "quad precision", mentioned in Section 2.5. With quad precision, the initial size of the constraint violation is many orders of magnitude smaller than in the standard "double precision" case. Our numerical evolutions show that this stays true for the whole evolution in particular because the machine round-off errors, which would otherwise dominate for $N = 300$ and sufficiently high time resolution, are much smaller. Now, since the results presented in Section 3.2 are virtually unchanged when they are repeated with quad precision, we conclude that these results are reliable despite the apparently large violation of the constraints at late times. Concerning the violation of the full Einstein's field equations, hence including all constraints and evolution equations, the same arguments lead to similar conclusions; consider Fig. 11.

Let us point the attention of the reader to Fig. 12, in order to show the order of magnitude of the violation of the smoothness conditions at the coordinate singularities. As we do not show here, these errors converge to zero, as long as the pure numerical

errors are not dominated by machine round-off errors. We note that none of the runs presented here enforce these smoothness conditions explicitly; it is possible that this would improve the numerical accuracy slightly [6].

4 Summary and outlook

In this paper, we studied the instability (non-genericity) of the Nariai solutions for the family of Gowdy perturbations. The investigations here are based on the first paper [5]. Our motivations to do this were two-fold. First, we were interested in the fundamental question of cosmic no-hair and its dynamical realization in more general classes than the spatially homogeneous case considered in [5]. Second, the results of the first paper suggest that the understanding of the instability of the Nariai solutions in the spatially homogeneous case could be exploited in order to construct cosmological black hole solutions with in principle arbitrarily complicated combinations of black hole and cosmological regions. Indeed, this interesting possibility was already considered in the spherically symmetric case in [7], where the author claims that such constructions are possible. Since no non-trivial cosmological black hole solutions are known for Gowdy symmetry with spatial $\mathbb{S}^1 \times \mathbb{S}^2$-topology to our knowledge, it was our aim to address this open problem.

Our results, which are obtained with the numerical technique introduced in [6], are as follows. First, by making experiments with various choices of perturbations, indeed more than those presented in this paper, we can confirm the expected instability of Nariai solutions, and hence the cosmic no-hair conjecture also in the case of Gowdy symmetric perturbations of the Nariai solution. That is, either the solutions close to a Nariai spacetime collapse in a given time direction, or when they expand, they form a smooth conformal boundary and hence are consistent with the cosmic no-hair picture. Hence, our results can be seen as a generalization of the work in [5] on the one hand. However, of even stronger interest is that our numerical results suggest that it is *not* possible to construct cosmological black hole solutions with small Gowdy symmetric perturbations of the Nariai solutions. This result is unexpected, in particular it is contrary to the claims for spherical symmetry. We find that the early time behavior agrees with the expectations. But then, the quantity H_2 starts to level off and the solution makes a decision, whether to either expand or collapse *globally* in space. The underlying mechanism is not understood. Of particular interest for future research will be the construction and study of the critical solution and of possible critical phenomena. One promising approach for shedding further light on these issues is to linearize the problem, on the one hand around the unperturbed Nariai solution, and on the other hand around the hypothetical critical solution.

Certainly, our class of initial data cannot be considered as "generic", or to put it the other way around, it is not clear how "special" it is. Thus it is hard to make predictions for general solutions close to generalized Nariai spacetimes. We are currently working on a method to obtain "general" Gowdy symmetric initial data numerically. General Gowdy initial data would allow us to study generalized Nariai solutions in particular in

the standard case $\sigma_0 > 0$. In this light, we understand our results here as first steps in an ongoing research project.

Since we find that it does not seem to be possible to construct cosmological black hole solutions by means of small Gowdy symmetric perturbations of Nariai data, it is natural to investigate large perturbations as a next step. The hope is that the spatially local behavior, which is suppressed in the case of small perturbations apparently, becomes significant. Beyond what we have presented in this paper here, our preliminary results suggest that this is the case. This will be investigated in another future publication.

We have discussed numerical errors and given some evidence that our numerical results are reliable. However, there is certainly room for improvements, not only in the numerical techniques, but also in the choice of gauge and the particular formulation of the field equations. For instance, in [4], we have interpreted the fact that we do not see spatially local behavior close to the singularities in our runs, so-called Gowdy spikes [1], as a reflection of the "bad" features of the Gauss gauge. That is, in this gauge, the solution approaches the singularity in a too inhomogeneous manner, obscuring such small scale structure. Hence, other gauge choices should be investigated. Another problem, already addressed before, is that our particular evolution system does not show optimal constraint propagation. Other formulations of the system should be tried and "constraint damping terms" should be investigated in order to improve this problem. Nevertheless, we have concluded above that our current numerical results can be trusted despite the apparently large constraint violations.

5 Acknowledgments

This work was supported in part by the Göran Gustafsson Foundation, and in part by the Agence Nationale de la Recherche (ANR) through the Grant 06-2-134423 entitled Mathematical Methods in General Relativity (MATH-GR) at the Laboratoire J.-L. Lions (Université Pierre et Marie Curie). Some of the work was done during the program "Geometry, Analysis, and General Relativity" at the Mittag-Leffler institute in Stockholm in fall 2008. I would like to thank in particular Helmut Friedrich and Hans Ringström for helpful discussions and explanations.

Appendix A Relation of the $\mathbf{U}(1) \times \mathbf{U}(1)$-actions on $\mathbb{S}^1 \times \mathbb{S}^2$ and $\mathbb{S}^3$

Let us consider a smooth global effective action of the group $\mathrm{U}(1) \times \mathrm{U}(1)$ on a 3-dimensional manifold. One can show, see the references in [9], that the only compatible smooth compact orientable 3-manifolds are $\mathbb{T}^3$, $\mathbb{S}^1 \times \mathbb{S}^2$, $\mathbb{S}^3$ and lens spaces. Since the universal cover of the lens spaces is $\mathbb{S}^3$, they will always be included when we speak about $\mathbb{S}^3$. In this paper, we are particularly interested in the case $\mathbb{S}^1 \times \mathbb{S}^2$. However, for the discussion of our numerical approach, which was worked out for the $\mathbb{S}^3$-case originally, it makes sense to consider the case $\mathbb{S}^3$ simultaneously now. On $\mathbb{S}^1 \times \mathbb{S}^2$, let us consider

coordinates (ρ, θ, ϕ) where $\rho \in (0, 2\pi)$ is the standard parameter on $\mathbb{S}^1$ and (θ, ϕ) are standard polar coordinates on $\mathbb{S}^2$

$$x_1 = \sin\theta\cos\phi, \quad x_2 = \sin\theta\sin\phi, \quad x_3 = \cos\theta. \tag{A.1}$$

In writing these coordinate expressions, we assume that $\mathbb{S}^2$ is embedded in the standard way into $\mathbb{R}^3$ with Cartesian coordinates (x_1, x_2, x_3). On $\mathbb{S}^3$, we consider Euler coordinates $(\chi, \lambda_1, \lambda_2)$ with the same conventions as in [4], namely

$$\begin{aligned} x_1 &= \cos\frac{\chi}{2}\cos\lambda_1, \quad x_2 = \cos\frac{\chi}{2}\sin\lambda_1, \\ x_3 &= \sin\frac{\chi}{2}\cos\lambda_2, \quad x_4 = \sin\frac{\chi}{2}\sin\lambda_2, \end{aligned} \tag{A.2}$$

where we assume the standard embedding of $\mathbb{S}^3$ into $\mathbb{R}^4$ similar to the above. Here, $\chi \in (0, \pi)$ and $\lambda_1, \lambda_2 \in (0, 2\pi)$. In terms of these coordinates on $\mathbb{S}^1 \times \mathbb{S}^2$ and $\mathbb{S}^3$, respectively, we can write a representation of the action of the group $G = \mathrm{U}(1) \times \mathrm{U}(1)$. For $\mathbb{S}^1 \times \mathbb{S}^2$, one has

$$\Psi : G \times (\mathbb{S}^1 \times \mathbb{S}^2) \to \mathbb{S}^1 \times \mathbb{S}^2, \quad ((u_1, u_2), (\rho, \theta, \phi)) \mapsto (\rho + u_1, \theta, \phi + u_2)$$

for $(u_1, u_2) \in \mathrm{U}(1) \times \mathrm{U}(1)$ and $(\rho, \theta, \phi) \in \mathbb{S}^1 \times \mathbb{S}^2$. In writing this, we always assume the standard identification of the groups $\mathrm{U}(1)$ and $\mathbb{S}^1$. Hence a basis of generators of the action are the coordinate fields ∂_ρ and ∂_ϕ. These are globally smooth vector fields on $\mathbb{S}^1 \times \mathbb{S}^2$ and one can check that this action is global, smooth and effective. The action degenerates at those points where the vector field ∂_ϕ has a zero, namely at the poles of the $\mathbb{S}^2$-factor given by $\theta = 0, \pi$. In the case of $\mathbb{S}^3$, we have the following action

$$\Psi : G \times \mathbb{S}^3 \to \mathbb{S}^3, \quad ((u_1, u_2), (\chi, \lambda_1, \lambda_2)) \mapsto (\chi, \lambda_1 + u_1, \lambda_2 + u_2).$$

The generators of the group are the coordinate fields ∂_{λ_1} and ∂_{λ_2}. Here, as well, these are globally smooth vector fields on $\mathbb{S}^3$. Indeed, the action is global, smooth and effective. The action degenerates where either ∂_{λ_1} or ∂_{λ_2} have a zero, which is the case at $\chi = 0, \pi$. Now, it is a fact, quoted in [9], that all other smooth effective global actions of $\mathrm{U}(1)\times\mathrm{U}(1)$ on any of these manifolds must be equivalent, i.e. can only differ by an automorphism of the group or by a diffeomorphism of the manifold to itself. Hence it is sufficient to have a single representation of the action.

We will now formulate the actions above in an equivalent, but more geometrical manner. We note that the fields W_1, W_2, W_3 defined in Eqs. (2.13), together with

$$\xi_3 := \partial_\rho,$$

form a basis of the Killing algebra in the spatially homogeneous case on $\mathbb{S}^1\times\mathbb{S}^2$. Moreover, the action of the group $\mathrm{U}(1) \times \mathrm{U}(1)$ is generated by $\{W_3, \xi_3\}$, i.e. the translation vector field along the $\mathbb{S}^1$-factor of the manifold and a rotation of the $\mathbb{S}^2$-factor of the manifold

corresponding to an element of the Lie algebra of SO(3). In the $\mathbb{S}^3$-case, let us introduce the vector fields

$$\begin{aligned}
Y_1 &= 2\sin\rho_1\,\partial_\chi + 2\cos\rho_1\,(\cot\chi\,\partial_{\rho_1} - \csc\chi\,\partial_{\rho_2})\,, && \text{(A.3a)}\\
Y_2 &= 2\cos\rho_1\,\partial_\chi - 2\sin\rho_1\,(\cot\chi\,\partial_{\rho_1} - \csc\chi\,\partial_{\rho_2})\,, && \text{(A.3b)}\\
Y_3 &= 2\partial_{\rho_1}\,, && \text{(A.3c)}\\
Z_1 &= -2\sin\rho_2\,\partial_\chi - 2\cos\rho_2\,(\cot\chi\,\partial_{\rho_1} - \csc\chi\,\partial_{\rho_2})\,, && \text{(A.3d)}\\
Z_2 &= 2\cos\rho_2\,\partial_\chi - 2\sin\rho_2\,(\cot\chi\,\partial_{\rho_1} - \csc\chi\,\partial_{\rho_2})\,, && \text{(A.3e)}\\
Z_3 &= 2\partial_{\rho_2}\,, && \text{(A.3f)}
\end{aligned}$$

in terms of the Euler angle coordinates above, but with ρ_1 and ρ_2 defined by

$$\lambda_1 = (\rho_1 + \rho_2)/2, \quad \lambda_2 = (\rho_1 - \rho_2)/2. \tag{A.4}$$

The definitions of these fields are in agreement with the conventions in [6, 4]. These vector fields have the property that they are globally smooth on $\mathbb{S}^3$ and are invariant under the standard left- and right-actions, respectively, of the group SU(2) on $\mathbb{S}^3$. Furthermore, they satisfy

$$[Y_a, Y_b] = 2\sum_{c=1}^{3}\eta_{abc}Y_c, \quad [Z_a, Z_b] = 2\sum_{c=1}^{3}\eta_{abc}Z_c, \quad [Y_a, Z_b] = 0.$$

Here η_{abc} is the totally antisymmetric symbol with $\eta_{123} = 1$. Note that the collections $\{Y_1, Y_2, Y_3\}$ and $\{Z_1, Z_2, Z_3\}$ are global frames on $\mathbb{S}^3$. A basis of the generators of the $\mathrm{U}(1) \times \mathrm{U}(1)$-action on $\mathbb{S}^3$ is $\{Y_3, Z_3\}$. We remark that both Y_3 and Z_3 are nowhere vanishing vector fields. They become, however, collinear at $\chi = 0, \pi$, and the $\mathrm{U}(1)\times\mathrm{U}(1)$-action degenerates.

Now, recall that both $\mathbb{S}^1\times\mathbb{S}^2$ and $\mathbb{S}^3$ are principal fiber bundles over $\mathbb{S}^2$ with structure group U(1). In the $\mathbb{S}^1 \times \mathbb{S}^2$-case, it is the trivial bundle with bundle map

$$\Phi_1 : \mathbb{S}^1 \times \mathbb{S}^2 \to \mathbb{S}^2, \quad (p, q) \mapsto q.$$

In the $\mathbb{S}^3$-case, it is the Hopf bundle and the bundle map can be given the representation

$$\begin{aligned}
\Phi_2 : \mathbb{S}^3 \to \mathbb{S}^2, &\quad (x_1, x_2, x_3, x_4) \mapsto (y_1, y_2, y_3)\\
&= (-2(-x_1x_3 + x_2x_4), 2(x_2x_3 + x_1x_4), x_1^2 + x_2^2 - x_3^2 - x_4^2).
\end{aligned}$$

Here the notation is such that $(x_1, x_2, x_3, x_4) \in \mathbb{S}^3 \subset \mathbb{R}^4$ with standard Cartesian coordinates on $\mathbb{R}^4$, and $(y_1, y_2, y_3) \in \mathbb{S}^2 \subset \mathbb{R}^3$. When we write this map in terms of the Euler angle coordinates for $\mathbb{S}^3$, given by Eqs. (A.2) and (A.4), and polar coordinates on $\mathbb{S}^2$ given by Eq. (A.1) (with x_i substituted by y_i), then the Hopf map has the simple representation

$$\Phi_2 : (\chi, \rho_1, \rho_2) \mapsto (\theta, \phi) = (\chi, \rho_1).$$

In order to simplify the notation we write now

1. N for $\mathbb{S}^1 \times \mathbb{S}^2$ or $\mathbb{S}^3$,

2. η for ξ_3 or Z_3, and σ for $2W_3$ or Y_3,

3. Φ for Φ_1 or Φ_2,

in the following. Furthermore, we write $G = \mathrm{U}(1) \times \mathrm{U}(1)$, and $G_1 = \mathrm{U}(1)$ to denote the subgroup of G generated by η. Recall that η is nowhere vanishing and note that its integral curves are closed circles. We notice that in both cases, the field η is tangent to the fibers of the bundles, and hence G_1 becomes the structure group, so that $N/G_1 \cong \mathbb{S}^2$. Note that, in particular, $\Phi_*\sigma$ is a smooth global vector field on $\mathbb{S}^2$, and indeed equals the coordinate vector field $2\partial_\phi$. This fact holds irrespective of the choice of either $\mathbb{S}^1 \times \mathbb{S}^2$ or $\mathbb{S}^3$, and thus clearly demonstrates how similar the two cases are at this level.

The bundle maps Φ can be used as follows. Assume that we want to solve a set of partial differential equations on N, possibly with an additional time function t. We suppose that all unknowns and coefficients are smooth functions on N constant along η, and that all differential operators in the equations originate in smooth vector fields on N whose Lie brackets with η vanish. Then it turns out that there is an equivalent system of equations on $\mathbb{S}^2$ as follows. Each such unknown and coefficient can be identified uniquely with a smooth function on $\mathbb{S}^2$ by means of the bundle map Φ. Furthermore, each such vector field yields a unique smooth vector field on $\mathbb{S}^2$ (which certainly has zeroes) when pushed forward with Φ. Most importantly, the solution of these new equations on $\mathbb{S}^2$, if it exists, hence yields a unique corresponding solution of the original problem on N. Thus without loss of information, we are allowed to "transport such geometric problems from N to $\mathbb{S}^2$" along the bundle map Φ.

References

[1] L. Andersson. The global existence problem in general relativity. In P.T. Chruściel and H. Friedrich, editors, *The Einstein Equations and the Large Scale Behavior of Gravitational Fields: 50 Years of the Cauchy Problem in General Relativity*, pages 71–120. Birkhäuser, Basel, Switzerland; Boston, U.S.A., 2004.

[2] L. Andersson and G.J. Galloway. dS/CFT and spacetime topology. *Adv. Theor. Math. Phys.*, 6:307–327, 2002, hep-th/0202161.

[3] F. Beyer. *Asymptotics and singularities in cosmological models with positive cosmological constant*. PhD thesis, Max Planck Institute for Gravitational Physics, Sep. 2007, gr-qc/0710.4297.

[4] F. Beyer. Investigations of solutions of Einstein's field equations close to λ-Taub-NUT. *Class. Quant. Grav.*, 25:235005, 2008, arXiv:0804.4224 [gr-qc].

[5] F. Beyer. Non-genericity of the Nariai solutions: I. Asymptotics and spatially homogeneous perturbations. *Class. Quant. Grav.*, 26:235015, 2009, arXiv:0902.2531 [gr-qc].

[6] F. Beyer. A spectral solver for evolution problems with spatial S3-topology. *J. Comput. Phys.*, 228(17):6496 – 6513, 2009, arXiv:0804.4222 [gr-qc].

[7] R. Bousso. *Adventures in de Sitter space*, pages 539–569. The future of theoretical Physics and Cosmology, Nov. 2003, hep-th/0205177.

[8] J.M. Martín-García C. Gundlach. Critical phenomena in gravitational collapse. *Living Reviews in Relativity*, 10(5), 2007, lrr-2007-5.

[9] P.T. Chruściel. On space-times with $U(1) \times U(1)$ symmetric compact Cauchy surfaces. *Annals Phys.*, 202:100–150, 1990.

[10] A. Clausen and J. Isenberg. Areal foliation and AVTD behavior in T^2 symmetric spacetimes with positive cosmological constant. *J. Math. Phys.*, 48:082501, 2007, gr-qc/0701054.

[11] H. Friedrich. Einstein equations and conformal structure: Existence of anti-De Sitter-type spacetimes. *J. Geom. Phys.*, 17:125–184, 1995.

[12] H. Friedrich. *The Conformal Structure of Spacetime: Geometry, Analysis, Numerics*, chapter "Conformal Einstein Evolution". Lecture Notes in Physics. Springer, 2002.

[13] H. Friedrich. On the nonlinearity of subsidiary systems. *Class. Quant. Grav.*, 22(14):L77–L82, 2005, gr-qc/0504129.

[14] H. Friedrich and G. Nagy. The initial boundary value problem for Einstein's vacuum field equations. *Commun. Math. Phys.*, 201:619–655, 1999.

[15] D. Garfinkle. Numerical simulations of Gowdy spacetimes on $S^2 \times S^1 \times R$. *Phys. Rev. D*, 60(10):104010, Oct. 1999, gr-qc/9906019.

[16] G.W. Gibbons and S.W. Hawking. Cosmological event horizons, thermodynamics, and particle creation. *Phys. Rev. D*, 15(10):2738–2751, May 1977.

[17] R.H. Gowdy. Vacuum space-times with two parameter spacelike isometry groups and compact invariant hypersurfaces: Topologies and boundary conditions. *Ann. Phys.*, 83:203–241, 1974.

[18] C. Gundlach, J.M. Martín-García, G. Calabrese, and I. Hinder. Constraint damping in the Z4 formulation and harmonic gauge. *Class. Quant. Grav.*, 22:3767–3774, 2005, gr-qc/0504114.

[19] S.W. Hawking and I.L. Moss. Supercooled phase transitions in the very early universe. *Phys. Lett. B*, 110(1):35–38, 1982.

[20] Intel. Intel Fortran Compiler, http://www.intel.com/support/performancetools/.

[21] J. Isenberg and V. Moncrief. Asymptotic behavior of the gravitational field and the nature of singularities in Gowdy space-times. *Ann. Phys.*, 199:84–122, 1990.

[22] C. Lübbe and J.A. Kroon. On de Sitter-like and Minkowski-like space-times. *Class. Quant. Grav.*, 26:145012, 2009, arXiv:0903.3899 [gr-qc].

[23] H. Nariai. *Sci. Re. Tohoku Univ. Ser. 1*, 34(3):160, 1950.

[24] H. Nariai. On a new cosmological solution of Einstein's field equations of gravitation. *Gen. Rel. Grav.*, 31(6):963–971, 1999.

[25] W.H. Press, S.A. Teukolsky, W.T. Vetterlin, and B.P. Flannery. *Numerical Recipes in C.* Cambridge University Press, 2nd edition, 1999.

[26] H. Ringström. Existence of an asymptotic velocity and implications for the asymptotic behavior in the direction of the singularity in T^3-Gowdy. *Comm. Pure Appl. Math.*, 59(7):977–1041, 2006.

[27] H. Ringström. Strong cosmic censorship in T^3-Gowdy spacetimes. preprint, accepted in Ann. of Math., 2006, `http://www.math.kth.se/~hansr/`.

[28] F. Ståhl. Fuchsian analysis of $S^2 \times S^1$ and S^3 Gowdy spacetimes. *Class. Quant. Grav.*, 19:4483–4504, 2002, gr-qc/0109011.

[29] J. Wainwright and G.F.R. Ellis. *Dynamical Systems in Cosmology.* Cambridge University Press, 1997.